

Optimized loading of an optical dipole trap for the production of Chromium BECs.

G. Bismut^{1,2}, B. Pasquiou^{1,2}, D. Ciampini³, B. Laburthe-Tolra^{1,2}, E. Maréchal^{1,2}, L. Vernac^{1,2}, and O. Gorceix^{1,2}

¹ Université Paris 13, Laboratoire de Physique des Lasers, Institut Galilée, 99 Ave J.B. Clément, F-93430 Villetaneuse, France, ² CNRS, UMR 7538, 99 Ave J.B. Clément, F-93430 Villetaneuse, France, ³ CNISM UdR Pisa, Dipartimento di Fisica E. Fermi, Università di Pisa, Largo Pontecorvo 3, I-56127 Pisa, Italy

October 11, 2018

e-mail: etienne.marechal@univ-paris13.fr

Abstract We report on a strategy to maximize the number of chromium atoms transferred from a magneto-optical trap into an optical trap through accumulation in metastable states via strong optical pumping. We analyse how the number of atoms in a chromium Bose Einstein condensate can be raised by a proper handling of the metastable state populations. Four laser diodes have been implemented to address the four levels that are populated during the MOT phase. The individual importance of each state is specified. To stabilize two of our laser diode, we have developed a simple ultrastable passive reference cavity whose long term stability is better than 1 MHz.

PACS 03.75.-b; 34.50.-s; 37.10.De; 67.85.-d

1 Introduction

Ultracold atoms have found a large amount of applications ranging from Bose-Einstein condensation (BEC) to exquisitely accurate measurements. The achievement of BEC in ultracold dilute gases triggered a burst of activity devoted to the experimental investigation of various fundamental issues in quantum physics. Numerous experimental setups are operated to enlarge the field of applications of trapped ultracold atoms [1]. Most of these experiments are performed with samples of alkali atoms that are relatively easy to cool down to the micro-Kelvin range in magneto-optical traps (MOTs), and that can be evaporatively cooled down to the nanoKelvin range after their transfer into a magnetic trap (MT). The extension of the cooling techniques to other atoms is attractive for several reasons among which one can quote only an arbitrary selection while, of course, some atoms are pertaining to several classes of applications or scientific goals. Several atoms possessing more complex internal level structure than alkalis are appealing for optical frequency precision metrology (earth-alkali atoms like Calcium [2], Strontium [3] and Mercury [4]) or for testing ultracold collision theories [5]. Earth alkali atoms have also been proposed as quantum registers

[6]. Atoms that come along with a diversity of naturally abundant isotopes (such as Ytterbium and Chromium) are appealing in the prospect of producing and studying mixtures of fermionic and/or bosonic quantum degenerate gases [7]. Furthermore, group III atoms (like Aluminium, Gallium and Indium [8]) as well as Iron [9], have been optically manipulated in view of potential applications in nanofabrication. Finally, cooling of highly magnetic atoms opens the possibility to study the effect of dipole-dipole interactions in degenerated quantum gases. Among these atoms, Chromium atoms carry a magnetic moment of $6 \mu_B$, Erbium atoms of $7 \mu_B$ [10] and Dysprosium, recently laser cooled in a MOT [11], of $10 \mu_B$. Chromium BECs have been produced during the last five years in the group of T.Pfau at the Stuttgart University and in our group [12, 13]. This article is devoted to the optimization of the production of such a BEC using an all-optical procedure. Even though we concentrate on our specific atomic species, the techniques that we present to reach degeneracy and raise the number of condensed atoms, apply to many other experimental endeavors in which the handling of leaky transitions, the accumulation in metastable states and the need for an optimized loading into an optical trap are technical bottlenecks that need to be overcome.

In this paper, we precisely describe the loading of an optical dipole trap directly from a MOT. Metastable states are populated in a MOT by optical pumping, and are trapped in a single beam horizontal optical dipole trap. Thus, cooling in the MOT and trapping in metastable states become independent. This reduces light-assisted density-limiting processes, and allows for a larger density in the optical dipole trap, in the spirit of the dark spot physics [14]. We describe the optimization of the loading process by use of optical depumping towards four different metastable states. We find that the total number of atoms accumulated in metastable states is relatively independent of the metastable states in which the depumping is achieved, but most sensitive to the depumping rate. We find that optimum loading arises when the depumping timescale is comparable to the equilibration (or damping) time in the MOT. Such a strong depumping depletes the MOT atom number so that light assisted losses (particularly strong

in the case of Cr) becomes negligible and do not limit the loading efficiency anymore.

Another beneficial consequence of the strong depumping, is that by limiting the MOT density, it limits the rescattering of light, leading to MOTs of small size which nicely match the size of the optical dipole trap. This leads to a very good transfer rate of atoms from the MOT to the dipole trap, which is very hard to achieve with MOTs having a larger size. We also discuss the impact of this optimization on the BEC production. The Appendix describes an ultra-stable Fabry-Perot cavity, with very good long term stability, which we use to lock two laser diodes repumping two of the four metastable states involved.

2 Strategies for the creation of a Chromium BEC

Reaching quantum degenerate regime with chromium atoms is difficult, due to unfavorable collisional properties. Specific strategies had to be invented to tackle with particular magnetic and spectroscopic properties of chromium. An important particularity of chromium is that inelastic light assisted collision rates are abnormally high. As a consequence, chromium magneto-optical trap clouds are small, both in size and atom number, limited to less than 10^7 atoms. For example, the first MOTs to be obtained [15,16,17] were limited to 10^6 atoms. As shown in Fig. 1, laser cooling is realized using the almost closed strong ${}^7S_3 \rightarrow {}^7P_4$ transition at 425 nm. Atoms in the excited 7P_4 state can decay to the 5D_4 and 5D_3 metastable states with a branching ratio of the order of 10^{-5} . A natural idea is to plug these leaks by shining two lasers resonant with the transitions between these metastable states and the 7P_4 or 7P_3 state (due to stronger transition strengths, we repump the metastable atoms via the 7P_3 state). Even with these two repumpers on, the atom number in the MOT remains limited to a few 10^6 atoms because of light assisted collisions. Strategies to produce chromium BEC have to deal with this relatively small number of atoms in the MOT.

The metastable 5D levels offer a means to prepare large samples of cold atoms from a MOT. Indeed, as shown in figure 1 and stated above, atoms in 7P_4 state can decay to metastable levels 5D_4 and 5D_3 . If their internal magnetic number m_j is positive (i.e. if they are in a low field seeking state), they remain trapped by the magnetic field gradient produced by the MOT coils, while they are immune to the MOT light. In addition, as the magnetic moment of chromium atoms is as high as $6 \mu_B$ for the fully stretched states, chromium atoms are supported against gravity by moderate magnetic gradients compatible with the optimal MOT working point.

This continuous loading of the magnetic trap with metastable atoms is the first key step in the road leading to the achievement of the first chromium BEC [12, 18]. From this point, the strategy of the Stuttgart group is the following: they load a few 10^8 chromium atoms in a Ioffe-Pritchard (IP) magnetic trap, using only the 5D_4 level as a reservoir, the 5D_3 state being continuously repumped with a laser resonant with the ${}^5D_3 \rightarrow {}^7P_3$ transition. This IP magnetic trap is loaded from

a 2D-MOT trap that shares the same magnetic potential. After a Doppler cooling stage, necessary to increase the initial phase-space density, and a first evaporation stage in the magnetic trap, atoms are transferred into a dipole trap. Once the dipole trap is loaded, atoms are optically pumped into the lowest energy level (${}^7S_3, m_j = -3$), to overcome the inelastic dipolar relaxation processes [19], and the final evaporation ramp is performed in a 1D dipole trap and then in a crossed dipole trap. The whole evaporation procedure cannot be performed entirely in a magnetic trap because chromium exhibits large dipole-dipole inelastic collision rates that preclude the BEC formation [19]. The dipole-dipole collisions lead to relaxation of the initially magnetically trapped low field seeking state ($m_j = +3$) toward state of lower energy, which releases kinetic energy. To avoid this mechanism, atoms have to be trapped in the true fundamental state ($m_j = -3$), which cannot be trapped in a magnetic trap, so that a dipole trap has to be used.

In Villetaneuse, we follow a shortcut by directly loading a dipole trap with metastable atoms from the MOT, to bypass the intermediate loading stage of atoms into a Ioffe-Pritchard type magnetic trap. We have demonstrated that a one beam dipole trap can be efficiently loaded during the MOT phase [20]. For this setup, an horizontal dipole trap is focused at the position of a conventional MOT (comprising a quadrupolar magnetic field) so that metastable atoms accumulate in the combined magnetic plus dipole trap: atoms are trapped by dipolar forces transversally and by magnetic forces along the direction of the dipole trap beam. Our strategy to reach the quantum degeneracy involves, as a crucial point, the maximization of the number of atoms accumulated in this combined trap.

A first original idea was to cancel out the effect of the magnetic trap on metastable atoms during the accumulation stage using rf-sweeps. We have demonstrated that in presence of appropriate rf-sweeps, metastable atoms produced during the MOT phase accumulate in a *pure* dipole trap. The MOT is unaffected by the presence of the strong rf fields used during the rf-sweeps. This scheme allows to trap both the high-field and low-field seeker atoms in the dipole trap, and decreases the confinement along the trapping laser beam propagation axis. We have shown that this rf sweep scheme increases the number of atoms loaded in the dipole trap by 50 % [21]. A second decisive step was to force new leaks towards metastable levels by using a depumping laser, to increase the number of atoms initially loaded in the dipole trap. In particular, the accumulation in a new metastable state, 5S_2 , turned out to be a decisive step to reach BEC [13]. In the present paper, we quantify in details the contributions of the different metastable levels. This allows us to optimize the atom number in the BEC, using a procedure that enables the independent addressing of each of the metastable states that can be loaded from the MOT into the optical trap.

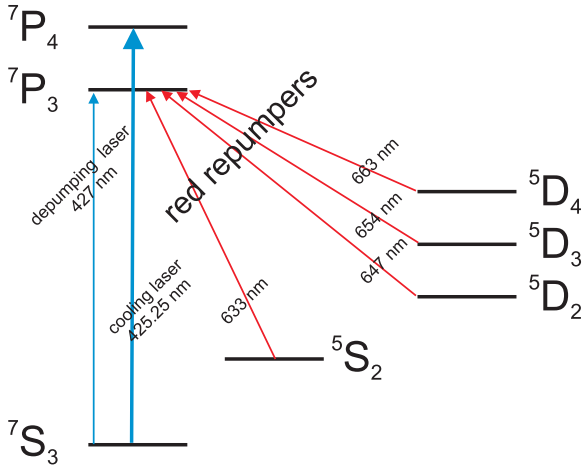


Fig. 1 Simplified Chromium energy scheme, showing the relevant levels and transitions. The strong ${}^7S_3 \rightarrow {}^7P_4$ transition at 425 nm is used for cooling. The ${}^7S_3 \rightarrow {}^7P_3$ transition at 427 nm is used for depumping, with a power of 80 μ W. Atoms accumulated in the four metastable states 5D_4 , 5D_3 , 5D_2 and 5S_2 can be repumped into the fundamental state using four independent red laser beams (with wavelengths between 633 and 663 nm.)

3 Metastable level scheme

As shown in Fig. 1, metastable states have to be taken into account when cooling Chromium. As already mentioned, when atoms are cooled using the ${}^7S_3 \rightarrow {}^7P_4$ transition at 425.6 nm, metastable states 5D_4 and 5D_3 are populated due to a weak coupling between these two states and the excited state 7P_4 . In addition, by exciting the 7P_3 state with a 'depumping' laser at 427.6 nm, two further metastable states become also populated: 5D_2 and 5S_2 . The couplings between these four metastable states and the two excited states 7P_4 and 7P_3 are listed in Tab. 1. These couplings remain small compared to the ones between the 7S_3 state and the two excited states 7P_4 and 7P_3 which are characterized by a transition rate $A = 3.1 \cdot 10^7 s^{-1}$ [22]. When only the main transition at 425 nm is excited, the branching ratio between transitions to the 5D_4 state and the 7S_3 state is of $4.1 \cdot 10^{-6}$. For this reason atoms have time to be efficiently cooled in the MOT before they decay into the metastable states. Coupling to the 5S_2 state is stronger than to the other metastable states, and atoms can be accumulated mostly in this state, in presence of the depumping laser, as demonstrated by the reported below experimental studies.

	7S_3	5S_2	5D_4	5D_3	5D_2
7P_4	$3.15 \cdot 10^7$	forbidden	127	42	forbidden
7P_3	$3.07 \cdot 10^7$	$2.9 \cdot 10^4$	$6 \cdot 10^3$	unknown	unknown

Table 1 Transition probabilities in s^{-1} (from the NIST Atomic and Spectra Database [22], and from [23]).

4 Loading of a dipole trap with metastable atoms

4.1 Experimental setup

Our setup to implement a dipole trap has been already presented in [13, 20]. An horizontal retroreflected infra-red (IR) laser beam (35 W max, $\lambda = 1075$ nm) is focused at the MOT position with a waist of 42 μ m. This far red detuned laser realizes a dipole trap into which cold metastable atoms accumulate. The four metastable levels can be addressed using four independent red laser beams (see Fig. 1), allowing to repump each metastable state through the 7P_3 excited state. We give in the appendix the technical details in relation to the frequency stabilization of these four repumping lasers. At the MOT position, these red laser beams have a power of typically 5 mW and a 1 mm $1/e^2$ radius. The sequence of accumulation is the following: at $t=0$, the MOT laser at 425 nm, the depumping laser at 427 nm and the trapping IR laser are switched on. For all these experiments, the IR laser power was set to 30 W. In addition, during the accumulation sequence, the rf-sweeps are always switched on. As explained above, metastable atoms accumulate therefore in a one-beam pure dipole trap [21]. As we have developed a laser setup that can address independently each metastable state, we can choose to accumulate into one single metastable state or into different states simultaneously by switching on or off the red laser addressing the corresponding state during the accumulation stage, as explained in the next subsection. When a given red laser is on, the leak to the corresponding metastable state is 'plugged'. After a given accumulation time, the MOT magnetic field, the MOT beams and the depumping 427 nm laser are switched off. The four red laser beams are switched on during 30 ms to repump all the metastable atoms into the fundamental state 7S_3 . Atoms are then polarized in the $m_j = -3$ state with a σ^- pulse resonant with the ${}^7S_3 \rightarrow {}^7P_3$ transition at 427 nm, in presence of a bias field of about 2 Gauss. Finally, the optical trap is switched off, and after a time of flight of typically 1 ms, the atom cloud is imaged by absorption imaging using a laser circularly polarized and resonant with the cooling transition at 425 nm.

4.2 Simultaneous or independent loading of the different reservoirs

We have studied the influence of the different repumpers on the accumulation of metastable atoms in the trap. A naive idea is that the number of accumulated atoms should raise if we increase the number of reservoirs. Nevertheless, for a given reservoir, loaded with only one given state, the maximum number of atoms in this reservoir is fixed by an equilibrium between the loading rate and inelastic collision rates. The loading rate is related to the transition probabilities tabulated in Tab. 1 and to the power of the cooling and depumping lasers, which sets the excited state population in 7P_3 and in 7P_4 . Inelastic collisions which limit the number of trapped

metastable atoms are of two types: light assisted inelastic collisions with 7P_4 and 7P_3 atoms and 2-body inelastic collisions between metastable atoms. When several reservoirs are loaded simultaneously, 2-body inelastic collisions between the different metastable states also occur. The optimization problem at stake is therefore complex, the number of parameters being large, and the interspecies inelastic collision rates between the metastable states being unknown. In Fig. 2 we show the comparison between the final number of atoms that can be loaded in the dipole trap when all the metastable states are populated during the accumulation phase (column a), and when only one of these reservoirs is filled during the accumulation phase, the other metastable states being continuously repumped (columns b to e). We obtain a surprising result : as shown by the first two columns, when one accumulates atoms in all the metastable states (column a) or only in the 5S_2 state (column b), the same final atom number is reached within the experimental error bars ($\approx 10\%$). In other words, we obtain the same final result if we repump the 5D_4 , 5D_3 and 5D_2 levels continuously or if we repump them only at the end of the accumulation phase thus effectively accumulating atoms in these states. The 5S_2 state is therefore a reservoir that allows simply by itself to optimize the trap loading, and is more favorable than any of the metastable 5D states. We will therefore focus on this particular state in the next two paragraphs. We also show on column a the population distribution of the different metastable states at the end of the accumulation, when the four channels are open. To perform this measurement, we have repumped only the measured channel at the end of the accumulation phase; the number of atoms accumulated in the ground state 7S_3 is obtained when we do not repump any metastable states. We observe that atoms are mainly loaded in 5S_2 , 5D_4 state and also in the fundamental state 7S_3 . Comparing columns b to e with column a show that for a given state, the number of accumulated atoms is maximized when the other states are not populated. If not, inelastic collisions with other metastable states increase the losses and lead to a smaller steady state atom number. Finally, we obtain that only very few atoms are accumulated in the 5D_2 state (column e). Indeed when all repumpers are on (column f), we obtain almost as many atoms as when all but the 647 nm repumpers are on. We therefore estimate that only 3.10^4 atoms are accumulated in the 5D_2 state to be compared to the 2.10^5 atoms accumulated directly in 7S_3 . This indicates that the coupling rate between 5D_2 and 7P_3 is very small.

A simple theoretical model can account for these experimental findings. We will show here that the experimental outcomes can be explained by assuming that depumping in metastable states is achieved in a timescale which is short compared to the timescale for light assisted losses in the MOT (as will be checked in next paragraph). We will also assume that the inelastic loss parameters for all different combinations of metastable states are all roughly equal. With these two only assumptions, simple rate equations account for the observation that accumulating only in the 5S_2 states while continuously repumping all other metastable states (column

b) leads to the same number of accumulated atoms than accumulating in all metastable states (column a).

For example, in case there are two metastable states, the rate equations read

$$\frac{dN_1}{dt} = N_{MOT}\Gamma_1 - \beta\frac{N_1}{V}N_1 - \beta\frac{N_2}{V}N_1 \quad (1)$$

$$\frac{dN_2}{dt} = N_{MOT}\Gamma_2 - \beta\frac{N_2}{V}N_2 - \beta\frac{N_1}{V}N_2 \quad (2)$$

$$\frac{dN_{MOT}}{dt} = \Gamma - N_{MOT}(\Gamma_1 + \Gamma_2) \quad (3)$$

where $N_{1,2,MOT}$ is the number of metastable atoms in states 1, 2 or in the MOT, β the inelastic loss parameter in metastable states, and V the effective trap volume. $\Gamma_{1,2}$ are the depumping rates into states 1 and 2. Γ is the loading rate of the MOT. Note that, when the light assisted collisions are not negligible, a new term has to be added to equations 1 to 3 of the form $\beta_{P-i}n_{MOT}^*N_i$ where n_{MOT}^* is the density of excited 7P_4 atoms, and β_{P-i} is the light assisted loss rate between atoms in 7P_4 state and atoms in state 1, 2 or the MOT atoms.

We solve this set of simple equations in two different cases. In the first case, we assume that metastable atoms 2 are continuously repumped, so that atoms only accumulate in state 1. The steady state for the MOT atom number is $N_{MOT} = \frac{\Gamma}{\Gamma}$, and the steady state for the metastable atom number is $N_1 = \sqrt{\frac{V\Gamma}{\beta}}$. In the second case, we continuously accumulate atoms in both metastable states, corresponding to a steady state situation $N_{MOT} = \frac{\Gamma}{\Gamma_1+\Gamma_2}$ and $N_1 + N_2 = \sqrt{\frac{V\Gamma}{\beta}}$.

This simple model (which can be easily extended to include the four metastable states) hence reproduces our main experimental observations: accumulating in all metastable states or in only the 5S_2 state (by continuously repumping all other metastable states) leads to the same final atom number. The reason for that is that depumping to the 5S_2 is so fast that inelastic losses can be neglected in the ground state, so that repumping all metastable states but one results in optical pumping to the state which is not repumped. The qualitative agreement between our observations and our simple model also indicates that the inelastic loss parameters corresponding to the different combinations of metastable atoms are of the same order of magnitude. The experimental results show nevertheless that, when we do not accumulate atoms in the 5S_2 state by repumping continuously this level with a repumper at 633 nm, we accumulate less atoms (columns c,d,e) in other states. This shows the limitations of our simple model: first, the 2-body loss rate parameter for 5D_4 state is twice bigger than for 5S_2 (as measured in subsection 4.4) leading to finally less atoms accumulated in this state (column c). Second, the depumping rates to the 5D_3 and 5D_2 states are very small so that in addition light-assisted collisions are no more fully negligible when we accumulate only in these states (column c and e).

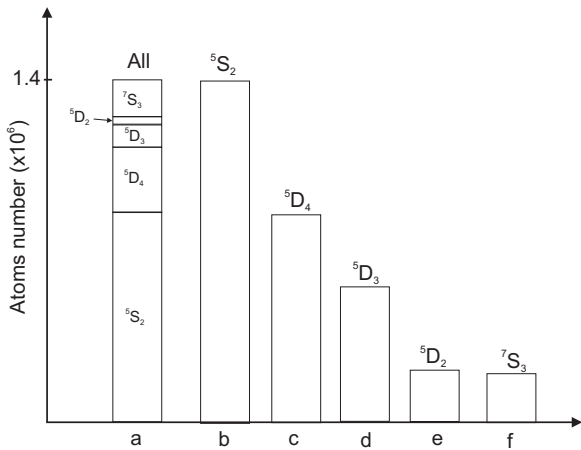


Fig. 2 Numbers of atoms in the dipole trap, after the accumulation and the repumping in the fundamental state 7S_3 . (a) simultaneous accumulation in all metastable states, and state composition. (b)-(e) : accumulation in a single reservoir, the other reservoirs being plugged during the accumulation phase. (f) Accumulation only in 7S_3 when all the reservoirs are plugged.

4.3 Optimization of the 5S_2 loading

In Fig. 3, we present the number of atoms accumulated in the dipole trap when only the 5S_2 state is loaded during the accumulation phase as a function of the power of the depumping laser (at 427 nm). This laser is circularly polarized, and is collimated with a $1/e^2$ radius of 1.5 mm at the output of an optical fiber and shone to the MOT. We observe a plateau of optimal values between 30 and 70 μW . If the depumping power is too small, there are few atoms in the excited 7P_3 state and the loading rate to the 5S_2 reservoir is too weak. The number of atoms increases with the depumping laser power until the saturation is reached. If the power is too strong, another phenomenon occurs. The MOT is affected by the depumping laser: we observe a decrease of the MOT fluorescence when the depumping laser power is raised. The optimum loading is reached when atoms have time to be cooled by the MOT before decaying into the metastable states. To estimate the cooling time in the MOT, T_{MOT} , we first accumulate atoms in metastable states in a magnetic trap (the dipole trap is switched-off). We then switch-on the MOT laser beams with the repumping lasers for an adjustable time and we measure the time evolution of the initially large volume of the magnetic trap toward the steady state MOT volume. We obtain a $1/e$ time evolution $T_{MOT} = 10$ ms. This time has to be compared to the time T_{depump} spent by atoms cycling in the MOT before being depumped. To measure T_{depump} , we monitor the MOT fluorescence change when we switch on the depumping laser. The MOT fluorescence steady level evolved within a time scale T_{depump} to a slightly lower value. For a power of 35 μW we measure a $1/e$ time constant of $T_{depump} = 5$ ms. These results confirm that the optimal loading is obtained when T_{depump} and T_{MOT} are of the same order of magnitude.

We also compare the depumping time T_{depump} to the time associated to light assisted collisions T_{Light} . We estimate this time by measuring the MOT lifetime, when all the repumpers are ON, and when we suddenly switch off the Zeeman slower beam. We measure $T_{Light} = 14$ ms. In presence of the depump-

ing beam, the MOT fluorescence is decreased by a factor of two so that we can estimate that $T_{Light} \approx 30$ ms. This time is six times larger than T_{depump} confirming that light assisted collisions are not limiting the loading of the dipole trap when accumulating in 5S_2 . Note however that if we accumulate in ${}^5D_{4,3,2}$, the timescale for depumping is raised by a factor of at least five so that light assisted collisions may then play a role and limit the atom number.

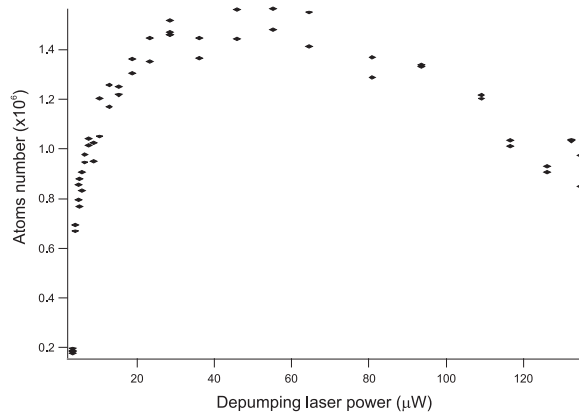


Fig. 3 Optimization of the number of atoms accumulated in the 5S_2 state in the dipole trap as a function of the depumping laser power. The atom number is measured after repumping in the fundamental 7S_3 state. The initial non zero value when the repumper is off corresponds to atoms directly loaded in the dipole trap from the MOT in the 7S_3 state.

4.4 Inelastic collisions in the 5S_2 state

The 5S_2 state is a particularly interesting reservoir, because our findings show that the loading is almost optimal when atoms accumulate only in this state. The loading rate through the coupling with the 7P_3 state is five times bigger for this state than for the 5D_4 state (Tab. 1, [22]) which favors the accumulation in this state. In the dipole trap, the number of accumulated atoms is limited by inelastic collision rates. We have therefore measured the 2-body inelastic collision rate β of this state. For this, we measured the decay of the 5S_2 atom number: once we have switched off the depumping and the MOT laser beams, we repump the 5S_2 state and take an absorption picture after a given time. During the decay, the density variation is locally governed by the following equation:

$$\frac{dn(\mathbf{r}, t)}{dt} = -\Gamma n(\mathbf{r}, t) - \beta n(\mathbf{r}, t)^2 \quad (4)$$

where Γ characterizes the one-body losses. In the present case, one body losses are mostly due to collisions with hot atoms coming from the thermal chromium beam, while in presence of the MOT beam light assisted collisions between atoms contribute also to the 1-body loss rate. We have checked experimentally that the shape of the atom density is well fitted by a Gaussian distribution, independent of time $n(r, t) =$

$\frac{N(t)}{V_0} e^{-\left(\frac{x^2}{x_0^2} + \frac{y^2}{y_0^2} + \frac{z^2}{z_0^2}\right)}$ where $V_0 = x_0 y_0 z_0 \pi^{3/2}$. In that case the solution of Eq. 4 can be integrated to give the evolution equation of the total atom number $N(t)$:

$$\frac{dN(t)}{dt} = -\Gamma N(t) - \frac{\beta}{2^{3/2} V_0} N(t)^2 \quad (5)$$

The solution of this equation is given by :

$$N(t) = \frac{N_0 e^{-\Gamma t}}{1 + \frac{\alpha N_0}{\Gamma} (1 - e^{-\Gamma t})} \quad (6)$$

where $\alpha = \frac{\beta}{2^{3/2} V_0}$ and $N_0 = N(t = 0)$. The observed non exponential decay is presented in Fig. 4. The fit to the data using Eq. 6 yields α , N_0 and Γ . The value of β is related to α with the relation $\beta = 2^{3/2} \alpha V_0 = 2^{3/2} \alpha N_0 / n_0$ where n_0 is the initial peak density. The direct measurement of the density by in situ absorption imaging is not possible as all the light is absorbed at the center of the cloud, leading to truncated absorption profiles. For this reason, we deduce the peak atomic density from measurements of the dipole trap beam parameters and by using the theoretical light shifts. The power of the optical trap laser is 2×30 W at the MOT position, the waist is $w_0 = 42$ μm and the estimated light shift is 12.9 MHz for the 5S_2 state. The theoretical calculation of this light shift is presented in [20]. The peak atomic density is then obtained by substituting a parabolic approximation to the dipole potential, and by considering a Maxwell Boltzmann distribution for the atom density in this potential. The temperature is measured by time of flight. For the conditions of Fig. 4 we found a temperature of 82 μK and we obtained a peak density of $1,30.10^{12}$ cm^{-3} giving a value of $\beta = 1,3.10^{-11}$ $\text{cm}^3 \cdot \text{s}^{-1}$. With additional measurements, we finally estimated a value of $\beta = 1,6.10^{-11} \pm 0,4.10^{-11}$ $\text{cm}^3 \cdot \text{s}^{-1}$. The main error comes from the estimate of the peak density. Using the same procedure, we measured the inelastic decay rate in the 5D_4 state to be $3,5.10^{-11}$ $\text{cm}^3 \cdot \text{s}^{-1}$. This value is in reasonable agreement with the already reported value of $2,6.10^{-11}$ $\text{cm}^3 \cdot \text{s}^{-1}$ and $3,3.10^{-11}$ $\text{cm}^3 \cdot \text{s}^{-1}$ [23,24]. We therefore conclude that the collisional properties of the 5S_2 state are slightly more favorable to accumulation than those of the 5D_4 state as β is about twice smaller for 5S_2 .

We also obtain that in the present case, the number of atoms loaded in the dipole trap is limited by two-body inelastic collisions between metastable atoms (as in [20]). This is very different from the case of the accumulation of metastable chromium atoms in a magnetic trap [23,25], where light assisted collisions between excited atoms 7P_4 from the MOT and metastable atoms are the dominant limiting mechanisms. This fact is clearly confirmed by the following experimental observation: when we measure the decay of the 5S_2 state presented in Fig. 4 in presence of the MOT, the initial decay, i.e. when the density is high, is unchanged. This also confirms that the simple model presented in subsection 4.2 is valid.

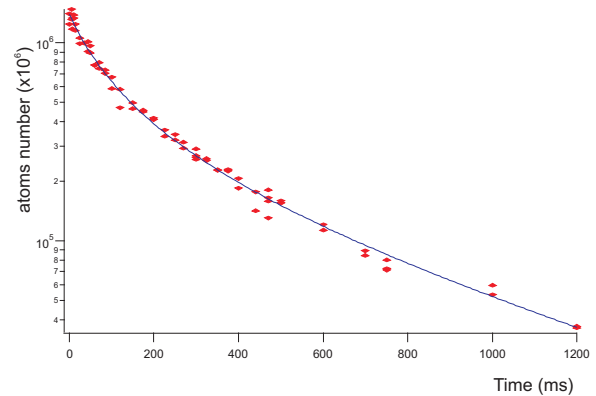


Fig. 4 Decay curve for the number of trapped 5S_2 atoms after the MOT and repumper beams have been switched off. The fit using Eq. 6 yields $\beta = 1,32.10^{-11}$ $\text{cm}^3 \cdot \text{s}^{-1}$ for the two-body loss coefficient (full line).

4.5 Relevance of the different metastable repumpers for the chromium BEC production

Before the conclusion, we sum up here our accumulation procedure for the production of the BEC (typically containing 15 to 20 thousand atoms in a pure condensate). As pointed out in sub-section 4.2, two equivalent procedures can be used to load efficiently the dipole trap, before starting the evaporation phase: either accumulating atoms in only 5S_2 or accumulating atoms in the four metastable channels (column a of Fig. 2). We use this last procedure: the repumping laser is switched-off during the accumulation phase, and are switched-on at the end to transfer all metastable atoms in 7S_3 . In addition, we add, as explained in [13], a 'dark spot' repumping laser during the accumulation phase, resonant on the $^5S_2 \rightarrow ^7P_3$ transition that continuously recycles 5S_2 atoms that are not in the dipole trap volume. This 'dark spot' laser (which was not used during the studies presented in this paper) allows to increase the final atom number in the BEC by 10%. We can finally estimate the relative importance of the different repumping lasers. In our case, if we do not repump atoms in the 5S_2 state at the end of the accumulation we obtain no BEC. If we do not repump 5D_4 atoms we decrease the BEC atom number by 78 %. And if we do not repump 5D_3 atoms, we decrease the BEC atom number by 25 %. Finally, as already mentioned previously, the repumping of the 5D_2 state has no effect on the final atom number on the BEC so that we do not use this repumping laser for the BEC production.

5 Conclusion

We have presented here our strategy to optimize the loading of a dipole trap for the production a chromium BEC. The dipole trap is directly loaded during the MOT phase and we optimized the loading by using a controlled depumping toward metastable states. We have shown that the depumping is strong enough to overcome the light-assisted limiting processes. The optimal depumping is obtained when the depumping rate is of the order of the MOT formation (damping) time T_{MOT} . We also focused on the relative relevance of the four

metastable states. We found that the 5S_2 state is more favorable than the other metastable states in view of raising the overall final number of trapped Cr atoms. We related this to the inelastic collision rate β of this state and compared its value to the one of the that states. We also found that the 5D_2 state is only very weakly coupled to 7P states so that it takes no part in the BEC production.

In the appendix, we have presented a method of stabilizing the frequency of laser diodes by locking them to a passive ultrastable Fabry-Perot cavity. The method requires very simple mechanics, optics and electronics. It could apply to many experiments in the ultracold atom physics domain.

Acknowledgments: LPL is Unité Mixte (UMR 7538) of CNRS and of Université Paris Nord. This research has been supported by Ministère de l'Enseignement Supérieur et de la Recherche (CPER) and by IFRAF (Institut Francilien de Recherche sur les Atomes Froids). G. Bismut acknowledges financial support by IFRAF. We thank the members of the HOTES group from LPL for giving us the ULE rod that we used to build the ultrastable cavity.

A Appendix: Description of the passive ultrastable cavity

The repumping lasers frequencies are generated by four independent extended cavity laser diodes delivering a power of 10 to 25 mW. To address the metastable states, each laser frequency has to be stabilized within 1 MHz to the corresponding chromium atomic transition.

For this purpose each laser's frequency is locked to an environmentally isolated Fabry-Perot stable cavity using the Pound Drever Hall (PDH) technique [26]. In brief, the laser beam is first split in two, the main power is used for the experiment and the other part is used for the lock. The laser current is gently modulated to a fixed frequency chosen between 10 and 20 MHz, through a bias T connected to the laser diode. This modulation gives rise to two main sidebands in the laser frequency spectrum. The reflected light from the Fabry-Perot cavity is detected on a fast photodiode. The phase sensitive detection at the modulation frequency gives the PDH dispersive error signal. This error signal is treated with a standard proportional integral differential regulator and then used to lock the laser frequency through the regulation of the laser current and of the piezo voltage of the diffraction grating of the extended cavity. With the PDH locking technique, many lasers can be locked on the same cavity, simply by assigning a different modulation frequency to each laser. For practical reasons, we have developed two distinct cavities to lock the four repumping lasers. The main difference between the two setups lies in the Fabry-Perot reference cavity.

For the first cavity, the cavity's length can be scanned by a PZT and locked to the $^7S_3 \rightarrow ^7P_4$ transition of ^{52}Cr by use of saturation spectroscopy. This set-up was developed in the early stages of the construction of our experience [17] and is used to lock the two diodes at 663 nm (5D_4 level) and at 633 nm (5S_2 level), corresponding to the two most important transitions. Indeed, with only these two diodes locked, we can produce a BEC. The Fabry-Perot cavity is first used to frequency stabilize the 851 nm Ti-Sapphire laser (from Tekhnoscan), pumped by a Verdi laser (from Coherent). The IR laser light is then frequency doubled in an external cavity at 425 nm. Finally, the Fabry-Perot cavity length is locked to the $^7S_3 \rightarrow ^7P_4$ transition using a saturated absorption in a chromium hollow cathode lamp. One important drawback of this setup is that the different feedback loops are highly intricate. If, for example, the Ti-Sapphire laser or the laser or the doubling cavity suddenly unlocks, the Fabry-Perot cavity is then no more referenced and locking of the repumping lasers has to be carried out again. As we have added two new red repumpers, we have decided to implement a passive reference cavity, whose length is therefore fixed in time and can be used everyday as a robust absolute frequency reference. We will describe here in more details the passive cavity, which is a simple versatile system that can be useful to many experiments where a long term stability is required.

The ultra-stable cavity scheme is shown in Fig. 5. The cavity is a degenerate confocal cavity, with a measured finesse of 82. The two converging spherical mirrors (curvature

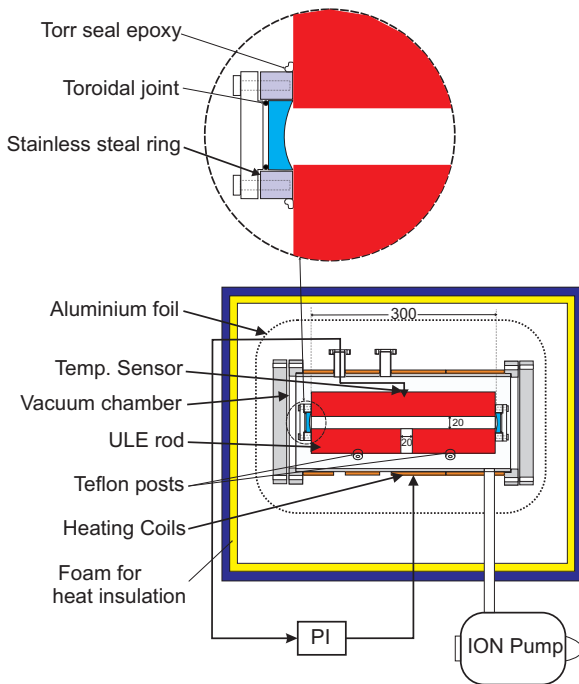


Fig. 5 Ultra-stable cavity set-up and detail of the mirrors fixing

radius of 300 mm) are fixed at the extremities of a Ultra Low Expansion (ULE) glass spacer, which defines the distance between the two mirrors. The mirrors fixing is shown in the inset of Fig. 5. A first ring (in stainless steel) is glued on the glass using Torr Seal epoxy. Another ring, screwed on the first, allows to gently push the mirror, through an helicoflex metallic joint, and put it in contact with the ULE rod. The ULE spacer (300 mm length, 100 mm diameter) has an axial aperture of 20 mm diameter for the laser beam propagation. It is also pierced in its center by a 20 mm hole for the pumping. The Fabry-Perot cavity is located inside an Ultra-High vacuum chamber pumped with a 10 l/s ion pump ($P < 10^{-8}$ mBar and rests on 4 teflon posts (2 mm diameter). In order to achieve the required temperature stability, heating coils are located around the external surface of the vacuum vessel containing the ULE rod. The heating coils are home made with a copper wire wined up around cardboard papers (pitch of 5 mm), which are then wrapped up around the vacuum chamber. This allows to have a uniform repartition of the heating foils at the vacuum vessel surface. A partially stable temperature environment is provided to the vacuum vessel by uniformly covering it with aluminium foils and by housing it in a thermal insulation box. The addition of the box reduces temperature fluctuations of the ULE rod by a factor 3. The temperature fluctuations and drifts are measured by placing several sensors (thermistors mounted on a Wheatstone bridge) on the surface of the vacuum vessel and inside it on the ULE rod. One of these sensors, which is stuck on the surface of the ULE rod, is giving the feedback signal for our Proportional-Integrator (PI) controller which acts upon the current sent through the heating coils. The thermal time constant of the ULE rod relative to the heating coils was measured to 8 hours, the coupling being mostly due to radiations

from the internal surface of the vacuum vessel. The temperature of the cavity is set to 26 °C, slightly above the room temperature. The room temperature is regulated to 23 °C with fluctuations less than $\pm 1^\circ$. The time constant of our PI corrector is set to 100 s so as to compensate for fast thermal fluctuations. In all cases it takes around 10 hours for the system to stabilize to a regime where the temperature at the measurement point on the surface of the ULE rod varies by less than 500 μ K. This temperature is measured by monitoring the error signal. We achieve a long term (1 year) stability below 1 MHz, tested using a frequency stabilized He-Ne laser at 633 nm. Using an AOM, the frequency of the laser light is swept over a free spectral range of the cavity and the position of the transmission peak of the laser light in the cavity is spotted at each frequency sweep. We could also daily check that the frequency of the cavity is stable, within 1 MHz, compared to the frequency of the ($^5D_3 \rightarrow ^7P_3$) repumping chromium transition at 654 nm.

During the development phase, we have measured the Coefficient of Thermal Expansion (CTE) of the whole cavity by ramping slowly the temperature of the ULE rod (3 days from 20 °C to 35 °C). Although a temperature dependence of CTE is recorded during measurements, a significant hysteresis on the temperature dependence of the cavity length is observed during the ramping up and down, which affects greatly the performances of the cavity in terms of sensitivity to temperature fluctuations. With our observations, a most reasonable assumption is that it stems from the frictions at the interface between the cavity and the teflon posts. Hysteresis makes every effort to reach a region of lower CTE useless. This induces a maximal CTE of $\alpha = 4,4 \cdot 10^{-7} K^{-1}$ at ambient temperature, which is at least 10 times worse than expected from such an ULE [27]. This relatively high CTE could be explained by the thermal expansion of the mirrors fixing system. Despite this hysteresis phenomenon, the very good performance of the temperature control allows us to reach the long term stability that is required. It must be noted that using the temperature sensor on the external surface of the vessel as the feedback branch for our frequency stabilization system did not provide a good enough screening of outside temperature fluctuations. Doing so, the frequency fluctuations has been measured to be around 6 MHz over 5 hours while the room temperature variation has been as large as 1K. We therefore concluded that for our setup, it was crucial to put the feedback sensor directly on the ULE rod surface.

We point out here that our cavity setup is remarkably simple. It uses standard electronics and optics (excepted the ULE rod, whose design is also simple). The cavity finesse is rather low, the fixation of the mirrors is basic. The obtained performances are far from the ones of very carefully designed high finesse ultrastable cavities developed in advanced labs [28]. Nevertheless our scheme for frequency stabilization is sufficient for most of the cold atoms experiments.

References

1. <http://www.uibk.ac.at/exphys/ultracold/atomtraps.html>.

2. S. Kraft, F. Vogt, O. Appel, F. Riehle, and U. Sterr. *Phys. Rev. Lett.*, **103**(13):130401, 2009.
3. S. Stellmer, M. K. Tey, B. Huang, R. Grimm, and F. Schreck. *Phys. Rev. Lett.*, **103**,200401 (2009).
4. M. Petersen, R. Chicireanu, S. T. Dawkins, D. V. Magalhães, C. Mandache, Y. Le Coq, A. Clairon, and S. Bize. *Phys. Rev. Lett.*, **101**(18):183004, 2008.
5. J. Weiner, V.S. Bagnato, S. Zilio, and P. S. Julienne. *Rev. Mod. Phys.*, **71**(1):1–85, Jan 1999.
6. A.J. Daley, M.M. Boyd, J. Ye, and P. Zoller. *Phys. Rev. Lett.*, **101**(17):170504, Oct 2008.
7. T. Fukuhara, S. Sugawa, Y. Takasu, and Y. Takahashi. *Phys. Rev. A*, **79**(2):021601, 2009.
8. S.J. Rehse, R.W. McGowan, and S.A. Lee. *Appl. Phys. B.*, **70**(657), 2000.
9. B. Smeets, R. W. Herfst, L. P. Maguire, E. te Sligte, P. van der Straten, H. C. W. Beijerinck, and K. A. H. van Leeuwen. *Appl. Phys. B.*, **80**(833), 2005.
10. A.J. Berglund, J.L. Hanssen, and J.J. McClelland. *Phys. Rev. Lett.*, **100**(11):113002, 2008.
11. M.Lu, S.H. Youn, and B.L. Lev. *Phys. Rev. Lett.*, **104**(6):063001, Feb 2010.
12. A. Griesmaier, J. Werner, S. Hensler, J. Stuhler, and T. Pfau. *Phys. Rev. Lett.*, **94**(16):160401, Apr 2005.
13. Q. Beaufils, R. Chicireanu, T. Zanon, B. Laburthe-Tolra, E. Marechal, L. Vernac, J.-C. Keller, and O. Gorceix. *Physical Review A (Atomic, Molecular, and Optical Physics)*, **77**(6):061601, 2008.
14. W. Ketterle, K.B. Davis, M.A. Joffe, A. Martin, and D.E. Pritchard. *Phys. Rev. Lett.*, **70**(15):2253–2256, Apr 1993.
15. A.S. Bell, J. Stuhler, S. Locher, S. Hensler, J. Mlynek, and T. Pfau. *Europhys. Lett.*, **45**(3):156, 1999.
16. C. C. Bradley, J. J. McClelland, W. R. Anderson, and R. J. Celotta. *Phys. Rev. A*, **61**(5):053407, Apr 2000.
17. R. Chicireanu, A. Pouderos, R. Barbé, B. Laburthe-Tolra, E. Maréchal, L. Vernac, J.-C. Keller, and O. Gorceix. *Phys. Rev. A*, **73**(5):053406, May 2006.
18. A. Griesmaier, J. Stuhler, T. Pfau. Production of a chromium bose-einstein condensate. *Appl. Phys. B*, **82**(211), 2006.
19. Q. Beaufils, A. Crubellier, E. Marchal, P. Pedri, L. Vernac, O. Gorceix, B. Laburthe-Tolra, B. Pasquiou, G. Bismut. arXiv:1002.0222v1, *Phys. Rev A* (in press), 2010.
20. R. Chicireanu, Q. Beaufils, A. Pouderos, B. Laburthe-Tolra, E. Marechal, L. Vernac, J. C. Keller, and O. Gorceix. *EPJD*, **45**(2):189, 2008.
21. Q. Beaufils, R. Chicireanu, A. Pouderos, W. de Souza Melo, B. Laburthe-Tolra, E. Marechal, L. Vernac, J. C. Keller, and O. Gorceix. *Phys. Rev. A*, **77**(5):053413, 2008.
22. Nist atomic spectra database.
23. J. Stuhler, P. O. Schmidt, S. Hensler, J. Werner, J. Mlynek, and T. Pfau. *Phys. Rev. A*, **64**(3):031405, Aug 2001.
24. R. Chicireanu, Q. Beaufils, A. Pouderos, B. Laburthe-Tolra, E. Marechal, J. V. Porto, L. Vernac, J. C. Keller, and O. Gorceix. *Phys. Rev. A*, **76**(2):023406, 2007.
25. P.O. Schmidt, S. Hensler, J. Werner, T. Binhammer, A. Axel Görlitz, and T. Pfau. *J. Opt. B: Quantum Semiclass. Opt.*, **5**:S170, 2003.
26. R. W. P. Drever, J. L. Hall, F. V. Kowalski, J. Hough, G. M. Ford, A. J. Munley, and H. Ward. *Applied Physics B: Lasers and Optics*, **31**(2), 1983.
27. T. George, H. W. Nicolaisen, A. Amy-Klein, C. Chardonnet V. Bernard, P. E. Durand. *IEEE journal of quantum electronics*, **31**(11):1913–1918, 1995.
28. J. Alnis, A. Matveev, N. Kolachevsky, Th. Udem, and T. W. Hänsch. *Phys. Rev. A*, **77**(5):053809, May 2008.